Differential and integral cross sections for electron elastic scattering by ammonia for incident energies ranging from 10 eV to 20 KeV

N. Sali and H. Aouchiche
Laboratoire de mécanique, structures et énergétique,
université Mouloud Mammeri de Tizi-Ouzou, B.P. 17, Tizi-Ouzou 15000, Algeria.
e-mail: h_aouchiche@yahoo.fr

Received 13 January 2018; accepted 4 April 2018

Differential and integral cross sections for elastic scattering of electron by NH_3 molecule are investigated for the energy ranging from 10 eV to 20 keV. The calculations are carried out in the framework of partial wave formalism, describing the target molecule by means of one center molecular Hartree-Fock functions. The potential used includes a static part -obtained here numerically from quantum calculation- and fine effects like correlation, polarization and exchange potentials. The results obtained in this model point out clearly the role played by the exchange and the correlation-polarization contributions in particular at lower scattering angles and lower incident energies. Both differential and integral cross sections obtained are compared with a large set of experimental data available in the literature and good agreement is found throughout the scattering angles and whole energy range investigated here.

Keywords: Electron-ammonia interaction; elastic scattering; correlation-polarization and exchange potentials; differential and integral cross sections.

PACS: 34.80.-i

1. Introduction

Electron collisions with NH_3 molecule are of prime interest in atomic and molecular processes in chemical reactions, collisions physics, interstellar space, atmosphere, radioactivity, plasmas (plasma etching, plasma deposition), switching device [1,2], biological matter and medicine. Ammonia is a colorless gas with a characteristic pungent smell; it is found in trace quantities in nature, being produced from the nitrogenous animal and vegetable matter, throughout the solar system, and in small quantities in rainwater. Ammonia is also known as caustic and hazardous in its concentrated form; it is currently used as fertilizer, cleaner, fuel, antimicrobial agent for food production, in fermentation, and textile. In addition, NH_3 is one of the important molecules considered as a source of nitrogen atoms for the fabrication of nitride films and other nitrogen compounds [3]. Considering these different domains of use, the e-NH_3 interaction has been the subject of many investigations in various energy ranges theoretically as well as experimentally.

On the experimental side, the absolute cross section of e-NH_3 interaction was measured first by Brüche in 1929 below 50 eV, using a Ramsauer-type apparatus [4], and then followed by the differential cross section (DCS) measurements reported by Harshbarger *et al*. (1971) [5] versus the momentum transfer between 2°-10° for 300, 400, and 500 eV, mentioning also unpublished data of Bromberg [6]. The measurements of the total cross sections (TCS) on NH_3 are renewed in 1987 by Sueoka *et al*. [7] using a linear transmission type time-of-flight apparatus from low to intermediate impact energies (0.7-400 eV). We also found the data reported by Szmytkowski *et al*. (1989) for impact energy from 1 to 80 eV, using a non-magnetic linear transmission technique [8]. Particularly, the results show a very broad hump centered around 10 eV. At the same time, Pritchard *et al*. [9] mentioned that Shyn has measured the relative DCSs for e-NH_3 interactions at 8.5 eV and 15 eV at intermediate and large angles [10]. The TCSs have been also measured in a transmission technique using a Ramsauer-type configuration in the 75-4000 eV energy range by Zeeca *et al*. (1992) [11]. At the same time, Alle *et al*. reported absolute TCS and DCSs measurements for vibrationally elastic electron scattering from NH_3 *et al* at incident energies 2-30 eV, using a crossed electron-molecular beam apparatus [12]. While in a wider energy range 300-5000 eV, Garcia and Manero (1996) used a method based on a transmission-beam technique including a detailed error-source analysis [13]. In another range of energy 400-4000 eV, Ariyasinghe *et al*. (2004) have measured the data from a linear transmission technique based on the electron-beam intensity attenuation through a gas [14]. Recently, Jones *et al*. (2008) reported the data in the low energy range 20 meV-10 eV including both integral scattering and scattering into the backward hemisphere with high energy resolution [15]. Furthermore, the elastic and inelastic scattering DCSs of high energy (35 keV) electrons scattered by NH_3 molecules were measured separately for the first time by Lahmam-Bennani *et al*. [16-17] and Dugu *et al*. [18], using two independent experimental methods. Finally, let us notice that many discrepancies exist between the cross sections produced in different laboratories. As mentioned by Karwazs *et al*. the most serious deviations arise in the TCS maximum resonant region (up to 25%), around 10 eV, and at high energies (to 35%) [19].

On the theoretical side, Itikawa (1971) adopted a general form of electron-molecule interaction in the Born approximation and derived a cross section formula for the rotational

transition in a symmetric-top molecule and applied it to the e-NH_3 collisions to evaluate the DCSs for energies lesser than 0.1 eV [20]. Many years later, Jain (1988) carried out calculation of the TCSs (elastic + inelastic) from 10 eV to 1000 eV, using a parameter-free spherical complex optical potential with different potential component models [21]. As the author mentioned, the results were so distinct that their comparison with the experimental data can help to select the model describing well the scattering process. At the same time, Benarfa and Tronc (1988) investigated the vibrational excitation and then calculated the DCSs and integral cross sections (ICS) at low energies (3-10 eV); particularly they analyzed the angular distributions of the elastic peak of the nv_1 series and of the v_4 vibrational mode [22]. Furthermore, Pritchard *et al*. (1989) reported differential and momentum transfer cross sections of elastic scattering for e-NH_3 collisions from 2.5 to 20 eV in the fixed-nuclei static-exchange approximation using the Schwinger variational principle [9]. Sometime later, Gianturco (1991) developed a model - to calculate the DCSs and ICSs for electron-NH_3 interactions - based on a free parameter correlation-polarization and exchange potentials, which play a fundamental role in describing the scattering of slow electrons from molecular targets [23]. In another calculation, Yuan and Zhang (1992) used the first-order Born approximation with the rotating molecule model, thus the total, differential, and momentum-transfer cross sections are reported for the vibrationally elastic scattering of electrons in the energy range 0.5-20 eV [24]. Besides, Rescigno *et al*. (1992) developed an ab-initio optical potential study using Kohn variational model including the static-exchange and polarized-self consistent-field of low-energy [25]. Their results demonstrate the sensitivity of the CSs to the short-range repulsion, long-range polarization, and the effects of the dipolar field particularly between 2 and 7.5 eV. Few years later, elastic and inelastic CSs for e-NH_3 interactions are also calculated in the energy range 50-200 eV by Joshipura and Patel (1996) using a modified additivity rule by separating e-molecule interactions into short-range and long-range parts [26]. Furthermore, Liu *et al*. (1997) have used the semi-empirical formula, complex optical potential, and the additivity rule in the intermediate and high energy range to evaluate the TCSs from 10 eV to 1 keV [27]. At the same time, Garcia and Manero (1997) used the empirical formula in the energy range 0.5-1 keV; their results reproduce sufficiently well (within 6%) their measurements for the series of investigated molecules (NH_3, CH_4, N_2, CO and CO_2) [28]. The DCSs are also obtained from 8.5 to 30 eV by Lino (2005) using the Schwinger variational principle [29]. As the Cartesian Gaussian functions basis - usually used in the method - is very effective only for short-range potentials, the authors introduced the plane waves as a trial basis set [29]. Recently, Munjal and Baluja (2006) reported also the DCSs, ICSs, momentum transfer, and excitation cross sections for the low-energy (0.025-20 eV) electron-NH_3 scattering, using the R-matrix method [30]. Few years later, Limbachya *et al*. proposed two different methods to calculate the rotationally elastic CSs for electron scattering from NH_3 attempting to demonstrate the possibility of producing robust cross sections over a wide energy range (0.01 eV to 2 keV) adaptable to any target [31]. The UK molecular R-matrix code through the Quantemol-N software package is used to calculate elastic plus electronic excitation cross sections for incident energies below the ionization threshold of the target, while at higher energies the spherical complex optical potential formalism was used [31]. Finally, note that the CSs for numerous polyatomic targets have been reviewed in these last decades by Shimamura [32], Hayashi [33], Morgan [34] and Karwazs *et al*. [19].

Despite the above-cited works, the differential and integral cross sections for electron elastic scattering by ammonia have not received all the attention merited. Regarding the works dedicated to the elastic scattering differential cross sections, they are very scarce in intermediate and higher energy range. Under these conditions, we propose in this paper to calculate elastic DCSs and ICSs for e-NH_3 molecule interactions in the energy ranging from 10 eV up to 20 keV. Furthermore, the spherical complex optical potential including static potential and the fine effects like correlation-polarization and exchange potentials are considered and their effects discussed. The static potential is obtained here numerically from quantum calculation using molecular wave functions determined by Moccia [35] while the correlation-polarization and exchange potentials are rigorously selected from the literature. In the following sections, atomic units (a.u.) are used everywhere.

2. Theoretical model

The calculations of differential cross section $d\sigma(\Omega))/d\Omega$ are developed in the coplanar geometry within partial wave formalism and non-relativistic approach, where Ω is the solid angle of the scattered electrons. Under these conditions $d\sigma(\Omega))/d\Omega$ can be given by the square of the scattering amplitude $f(\theta)$, whith

$$f(\theta) = \frac{1}{k}\sum_{l=0}^{\infty}(2l+1)e^{i\delta_l}\sin\delta_l P_l(\cos\theta), \qquad (1)$$

k is linked to the kinetic energy E by $2E = k^2, l$ the quantum number of the kinetic momentum, $P_l(\cos\theta)$ the Legendre polynomial and δ_l is the phase shift induced by the spherical potential $V(r)$ in the outgoing wave relatively to the free wave (for more details see Ref. 36). NH_3 being a pyramidal molecule with a heavy atom N, the charge distribution can be assumed as a spherical molecule centered at the nucleus N. Under these assumptions, the total potential $V(r)$ may be approximated by a spherical one including the static potential $V_{st}(r)$ and the two fine effects called polarization potential, $V_p(r)$, and exchange potential, $V_{ex}(r)$

$$V(r) = V_{st}(r) + V_p(r) + V_{ex}(r). \qquad (2)$$

2.1. Static potential

To evaluate the static potential, we use the ammonia molecular orbital functions determined by Moccia [35]. In this description, each molecular orbital was expressed in terms of Slater-type functions all centered at a common origin (the heaviest atom). Thus, the ammonia target can be described by means of $N_{\text{orb}}(N_{\text{orb}} = 5)$ molecular functions labeled $1A_1$, $2A_1$, $1A_3$, $1E_x$ and $1E_y$, written as [37]

$$\Psi_j(\mathbf{r}) = \sum_{k=1}^{N_j} a_{jk} R^{\xi_{ik}}_{n_{jk},l_{jk}}(r) S_{l_{jk},m_{jk}}(\hat{r}), \tag{3}$$

where N_j is the number of Slater functions used to construct the jth (with j varying from 1 to N_{orb}) molecular orbital $\Psi_j(\mathbf{r})$; $\hat{r}$ refers to the solid angle of the position vector $\mathbf{r}$, and a_{jk} the weight of each real atomic component. The function $R^{\xi_{ik}}_{n_{jk},l_{jk}}(r)$ represents the radial part expressed by Slater-type functions [38] as

$$R^{\xi_{ik}}_{n_{jk},l_{jk}}(r) = \frac{(2\xi_{jk})^{n_{jk}+1/2}}{\sqrt{(2n_{jk})!}} r^{(n_{jk}-1)} e^{-\xi_{jk}r}; \tag{4}$$

and the angular part $S_{l_{jk},m_{jk}}(\hat{r})$ are the real spherical harmonics linked to the complex form $Y_{l_{jk},m_{jk}}(\hat{r})$ by [39]

$$\begin{cases} S_{l_{jk},m_{jk}}(\hat{r}) = \left(\frac{m_{jk}}{2|m_{jk}|}\right)^{1/2} \left\{ Y_{l_{jk},-|m_{jk}|}(\hat{r}) + (-1)^{m_{jk}} \left(\frac{m_{jk}}{|m_{jk}|}\right) Y_{l_{jk},|m_{jk}|}(\hat{r}) \right\} & \text{if} \quad m_{jk} \neq 0 \\ S_{l_{jk},0}(\hat{r}) = Y_{l_{jk},0}(\hat{r}) & \text{if} \quad m_{jk} = 0 \end{cases} \tag{5}$$

For more details, we refer the reader to Refs. 35 and 37 where all the coefficients (a_{jk}, ξ_{jk}) and all quantum numbers (n_{jk}, l_{jk}, m_{jk}) used are reported. Besides note that the static potential includes electronic and ionic contributions

$$V_{st}(r) = [V^j_{st}(r)]_{elec} + [V^j_{st}(r)]_{ion}. \tag{6}$$

The electronic contribution is given for each molecular orbital j by

$$\begin{aligned}[V^j_{st}(r)]_{elec} = 2 \sum_{k=1,k'=1}^{N_j} & a_{jk} a_{jk'} \delta(m_{jk} - m_{jk'}) \\ & \times \delta(l_{jk} - l_{jk'}) \int_0^\infty R^{\xi_{ik}}_{n_{jk},l_{jk}}(r') \frac{r'^2}{r_>} \\ & \times R^{\xi_{ik'}}_{n_{jk'},l_{jk'}}(r') dr' \end{aligned} \tag{7}$$

and the ionic one by

$$[V^j_{st}(r)]_{ion} = -\frac{Z}{r} - \frac{1}{R_>}. \tag{8}$$

The symbols $r_>$ and $R_>$ are respectively given by $r_> = \max\{r, r'\}$, and $R_> = \max\{r, R_{NH}\}$ where $R_{NH} = 1.928$ a.u. [35] is the internuclear distance between the two atoms N and H, and $Z = 10$ for ammonia molecule.

2.2. Correlation-polarization potential

It is well established that NH_3 is polar covalent molecule due to the electronegativity difference between the nitrogen (higher) and the hydrogen atoms. Hence, e-NH_3 interactions induce an additive potential due to the polarizability of the target induced by the incident electrical charge particularly at low velocities. The polarization potential $V_p(r)$ used here refers to the well-known Buckingham type given by

$$V_p(r) = -\frac{\alpha_d}{2(r^2 + r_c^2)^2} \tag{9}$$

where α_d is the polarizability ($\alpha_d = 14.984$ a.u. for NH_3 [40]) and r_c is a cut-off-parameter expressed by Mittleman and Watson [41] as

$$r_c = \left(\frac{1}{2}\alpha_d z^{-1/3} b^2_{\text{pol}}\right)^{1/4}, \tag{10}$$

with b_{pol} an adjustable parameter. In our case, we found that (see Salvat *et al.* for more details [42])

$$b_{\text{pol}} = \sqrt{\max\{(E - 0.5)/0.01; 1\}} \tag{11}$$

where E refers to the incident electron energy.

As proposed by Salvat *et al.* [42], we use here the polarization potential combined with the correlation one, called correlation-polarization potential. Different expressions of the correlation potential are found in the literature; the first expression chosen here is given by Padial and Norcross (1981) [43]

$$\begin{cases} V_{c1}(r) = 0.0311 \log(r_s) - 0.0584 + 0.006 \log(r_s) - 0.015 r_s & \text{for} \quad r_s < 0.7 \\ V_{c1}(r) = -0.07356 + 0.02224 \log(rs) & \text{for} \quad 0.7 \leq r_s \leq 10 \end{cases} \tag{12}$$

and the second one is given by Carr and Maradudin (1964) [44]

$$\begin{cases} V_{c2}(r) = 0.0311\log(r_s) + 0.0584 - r_s(0.00133\log(r_s) - 0.0084) & \text{for} \quad r_s \leq 1 \\ V_{c2}(r) = -\beta_0 \frac{1+(7/6)\beta_1 r_s^{1/2}+(4/3)\beta_2 r_s}{(1+\beta_1 r_s^{(1/2)}+\beta_2 r_s)^2} & \text{for} \quad r_s \geq 1 \end{cases} \tag{13}$$

where $r_s = (3/4\pi\rho(r))^{1/3})$ and $\beta_0 = 0.1423$, $\beta_1 = 1.0529$ and $\beta_2 = 0.3334$. Following Salvat *et al*. [42] the correlation-polarization potential can be given by

$$V_{cp}(r) = \begin{cases} \max\{V_c(r), V_p(r)\} & \text{for} \quad r < r_{cr} \\ V_p(r) & \text{for} \quad r > r_{cr} \end{cases} ; \tag{14}$$

where r_{cr} is defined as the outer radius where the two potetials $V_p(r)$ and $V_c(r)$ cross.

2.3. Exchange potential

In addition to the polarization phenomena of the target in the electron-molecule interactions, the incident electron can be captured by the target - particularly at low incident energies - and then the latter releases one of their bound electrons. This phenomenon known as electron exchange process needs another potential called exchange potential. Among the various formulas available in the literature, we have selected two expressions; the first one $V_{ex1}(r)$, depending clearly on the static potential and the correlation-polarization one, was given by Furness and McCarty [45]

$$V_{ex1}(r) = \frac{1}{2}\Big\{E - (V_{st}(r)+V_{cp}(r)) - [(E-(V_{st}(r)+V_{cp}(r)))^2 + 4\pi\rho(r)]^{1/2}\Big\}, \tag{15}$$

where $\rho(r)$ is the spherical density of the electronic charge given by [45]

$$\rho(r) = \frac{1}{N_{orb}} \sum_{j=1}^{N_{orb}} \left| R^{\xi_{ik}}_{n_{jk},l_{jk}}(r) \right|^2 . \tag{16}$$

The second exchange potential $V_{ex2}(r)$, used here, was initially given by Mittleman and Watson [46] and re-written by Riley and Truhlar [47]:

$$V_{ex2}(r) = \frac{-1}{2\pi k_L}\Big\{k_L k_F - \frac{1}{2}\left(k_L^2 - k_F^2\right) \times Ln\left|\frac{k_L + k_F}{k_L - k_F}\right|\Big\} \tag{17}$$

where k_L is the local wave number of the electron projectile defined by $k_L^2 = k^2 + 2I^+ + k_F^2$, I^+ being the first ionization potential of the molecule target, $k_F(r) = (3\pi^2\rho(r))^{1/3}$ the Fermi wave number of the atomic electron cloud, and $k_2 = 2E$. For illustration, we have reported in Fig. 1 the various potentials used in this work and described above. In Fig. 1(a), the static potential - calculated according to Eqs. (6), (7) and (8) - decreasing rapidly up to large distances present a discontinuity around $r = 1.93\ a.u.$ due to the presence of the proton shell in the NH_3 molecule where the internuclear distance $R_{NH} = 1.928\ a.u.$ In panel (b), the two correlation-polarization potentials $V_{cp1}(r)$ and $V_{cp2}(r)$ are

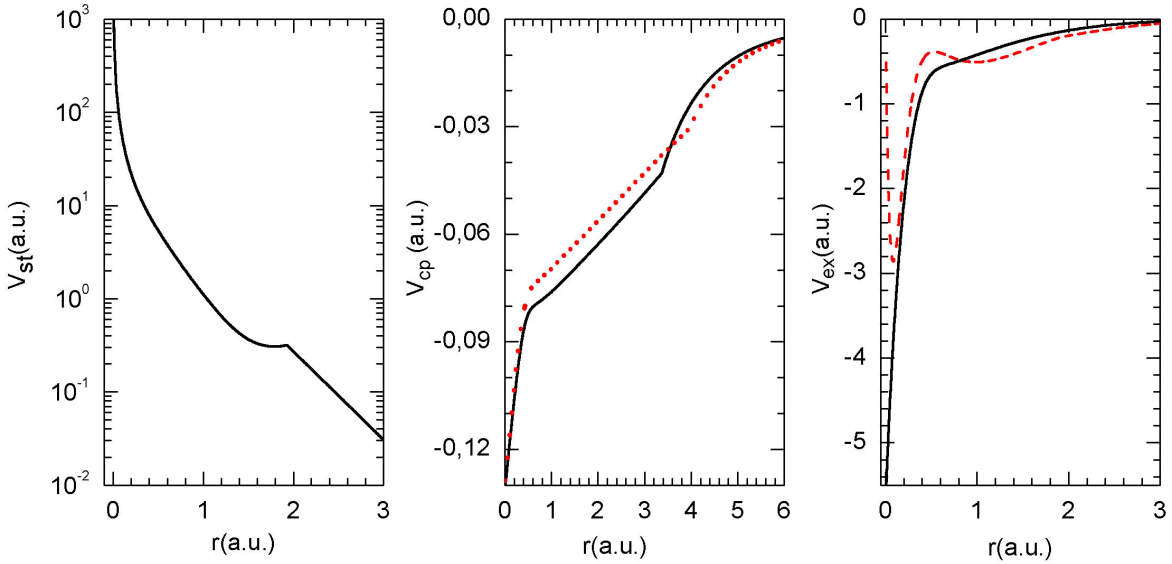

FIGURE 1. (Color online). Different potentials used in this work. (a) Static potentials used to describe the electron elastic scattering by ammonia molecules, (b) Correlation- polarization potentials V_{cp1} (black solid line) and V_{cp2} (red dotted line), (c) Exchange potentials V_{ex1} (black solid line) and V_{ex2} (red dashed line).

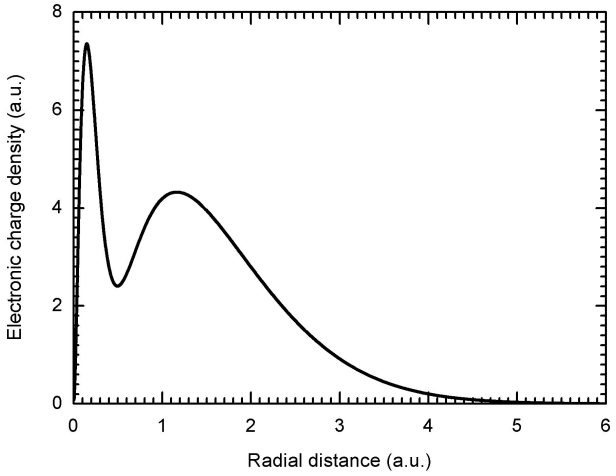

FIGURE 2. Electronic charge density of the ammonia molecule. The distance r refers to the center of the molecule, which is here merged with the heaviest atom center.

are compared, we clearly observe for $r < r_{cr}$ a quasi-linear behavior with the radius whereas they both mimic the asymptotic $V_p(r)$ potential and then depend on the projectile energy at large distances. The two exchange potentials $V_{ex1}(r)$ and $V_{ex2}(r)$ are reported in Fig. 1(c), the first one presents no minimum contrary to $V_{ex2}(r)$ which exhibits clearly a minimum for $r = 0.07\ a.u.$ However, they have nearly the same values at large distances r.

Finally, note that here we have studied studied two expressions for the correlation-polarization potential ($V_{cp1}(r)$ and $V_{cp2}(r)$) and two others for the exchange potential ($V_{ex1}(r)$ and $V_{ex2}(r)$). So, according to Eq. (2), we get four combinations for the potential $V(r)$, namely $V_{st}(r) + V_{cp1}(r) + V_{ex1}(r)$, $V_{st}(r) + V_{cp1}(r) + V_{ex2}(r)$, $V_{st}(r) + V_{cp2}(r) + V_{ex1}(r)$, and $V_{st}(r) + V_{cp2}(r) + V_{ex2}(r)$ which are used in our calculation.

3. Results and discussion

To evaluate the exchange potential (see Eq. (15)), we need, first, to calculate the electronic charge density, $\rho(r)$, of the ammonia molecule. Figure 2 reports the obtained electronic charge density versus the radius r accordingly to Eq. (16), using the molecular wave functions determined by Moccia [35]. The distribution exhibits two maxima located around 0.15 a.u. and 1.16 a.u, and one minimum around 0.5 a.u., as

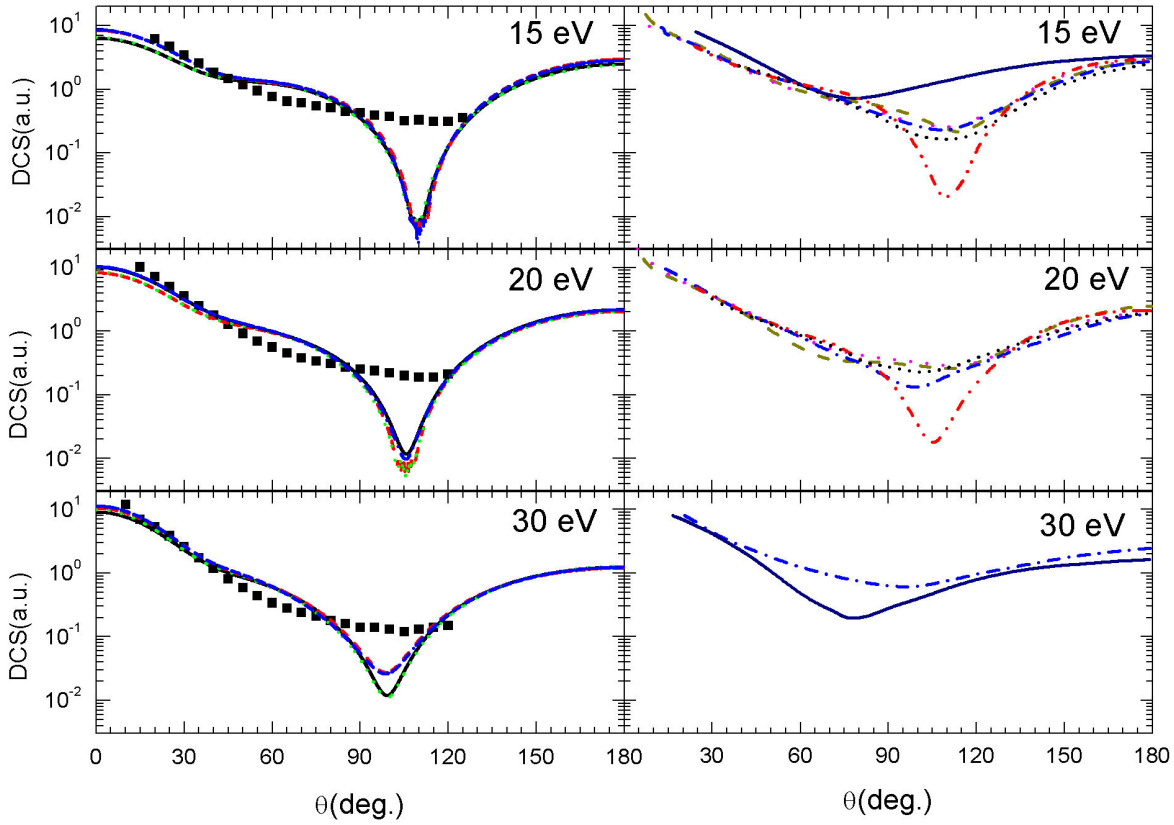

FIGURE 3. (Color online) In left panel: Comparison between calculated DCSs for electron elastic scattering by ammonia molecule at 15, 20, and 30 eV for various potentials: $V_{st}(r) + V_{cp1}(r) + V_{ex1}(r)$ (solid black line), $V_{st}(r) + V_{cp1}(r) + V_{ex2}(r)$ (dashed red line), $V_{st}(r) + V_{cp2}(r) + V_{ex1}(r)$ (dotted green line) and $V_{st}(r) + V_{cp2}(r) + V_{ex2}(r)$ (blue dash-dotted line). Experimental data are taken from [12] (black solid squares) and [10] (red open circles). In the right panel: theoretical results are taken from [9] (short-dashed black line), [23] (dash-dotted blue line), [24] (dash-dotted-dotted red line), [25] (dotted magenta line), [29] (solid navy line), and [30] (dashed dark-yellow line).

expected. The distribution shows no significant values over the radial distance $r = 6$ a.u. hence, the calculations can be achieved only in the range given by $0 \leq r \leq 6\ a.u.$

3.1. Differential cross sections

Differential cross sections for elastic scattering of electron by NH_3 molecule are calculated for scattering angles varying from 0 to 360° and for numerous incident energies. First, these differential cross sections are reported in Fig. 3 (left panel) for 15 eV, 20 eV and 30 eV, where experimental data are available and only from 0 to 180° since they are symmetrical with respect to the axis $\theta = 180°$. The calculations are carried out for the four above-cited combinations of potentials investigated in this work. To the best of our knowledge, the only existing experimental DCSs related to the energies investigated here, were reported by Alle *et al*. [12] and Shyn [10] and we are not aware of the existence of other measurements.

The DCSs obtained (left panel in Fig. 3) are important in the forward directions and lesser in the backward directions, while they are even smaller exhibiting a valley around the perpendicular directions, as expected. In general, the different exchange and correlation-polarization potentials, investigated here, provide quasi-identical DCSs and a good agreement is observed throughout the angle range for all the energies investigated. However, at lower scattering angles, the calculated DCSs exhibit little discrepancies particularly at lower energies. In fact, these discrepancies related to the form of the correlation-polarization potential considered are directly linked to the polar nature of the target since there is a mutual influence between the electric dipole of the molecule and the charge of the projectile. It is then evident that this influence, responsible of the discrepancies, became relatively important at lower incident energies, since the projectile spends a relatively important time near the target molecule. In addition, the DCS curves show the existence of a profound minimum, in the exhibited valley, whose depth depends on the form of the tested correlation-polarization and exchange potentials. The minima are located around $\theta = 109°$ at 15 eV which are shifted to lower scattering angles when the incident energy increases, namely around $\theta = 105°$ at 20 eV and around $\theta = 99°$ at 30 eV. Note that, outside the observed minima, our calculated DCSs are in excellent agreement with the experimental data reported by Alle *et al*. [12] for vibrationally elastic scattering (black full squares in Fig. 3), using a crossed electron-molecular beam apparatus [12]. Furthermore, our results are also in good agreement with the relative measures of Shyn [10] (red circles in Fig. 3)) mentioned and normalized at 90° by Pritchard *et al*. [9]. We would note that the profound minima exhibited in these calculated DCSs for elastic scattering by NH_3 are also found in our precedent works on H_2S [48] and HCl [49] at lower energies using the same model. Otherwise, in Fig. 3 (right panel) the theoretical DCSs taken from [29] (solid navy line), [30] (dashed dark-yellow line), [25] (dotted magenta line), [23] (dashed-dotted blue line), [24] (dashed dotted-dotted red line), [9] (short dashed black line) are also reported to compare with. Note that these DCSs do not show a profound minimum except that obtained by the Schwinger variational principle with plane waves [29] (dashed dotted-dotted red line at 15 eV and 20 eV) based on fixed-nuclei approximation. As already pointed out by Brescansin *et al* [50], these deep minima are probably due to the fact that only the spherical part of the interaction potential is considered in the calculations. Indeed, the spherical potential used here for describing the electron elastic scattering by the NH_3 molecule is quite similar to that of the Neon atom for which the numerous DCSs reported in the literature [51] clearly point out an identical depth at lower energies. We would note here, that at intermediate and relatively high energies these very deep minima disappear completely, as we will see below. We can conclude that they are non-physical structures and probably underline the limitation of the current spherical approach for modeling the elastic scattering process at lower energies.

In Fig. 4, we report the DCSs for electron elastic scattering at intermediate incident energies (300 eV, 400 eV, 500 eV, and 1 keV) for the four combinations of correlation-polarization and exchange potentials investigated in this work. These latter provide quasi-identical curves, and an overall agreement is observed in the whole angle range for all the energies investigated. The effects of the fine contributions (correlation-polarization and exchange potentials) no longer appear even in the range of lower scattering angles. Besides, the observed minima at low incident energies disappeared from the value of 200 eV (not reported here). In addition, we have reported in Fig. 4 the experimental data provided by Harsbarger *et al*. [5] (black solid squares) and by Bromberg [6] (red open circles) for the scattering angles from 2 to 10°. Our calculated DCSs appear slightly lesser than the experimental ones around 2° and seem to be in good agreement beyond this scattering angle value. Finally note that, to the best of our knowledge, there are no other results neither experimental nor theoretical in larger angle range to compare with.

3.2. Integral cross sections

Integral cross sections for electron elastic scattering from NH_3 molecules are also calculated using the four above-cited combinations including the static, correlation-polarization, and exchange potentials. The energy distribution for elastic scattering is obtained by integrating numerically the differential cross sections overall the scattering solid angle

$$\sigma(E) = 2\pi \int_0^{\pi} \frac{d\sigma(E,\theta)}{d\theta} \sin\theta d\theta. \tag{18}$$

The various obtained results are presented in Fig. 5a for the incident energies ranging from 10 eV to 20 keV, and for the four potential combinations investigated. As expected,

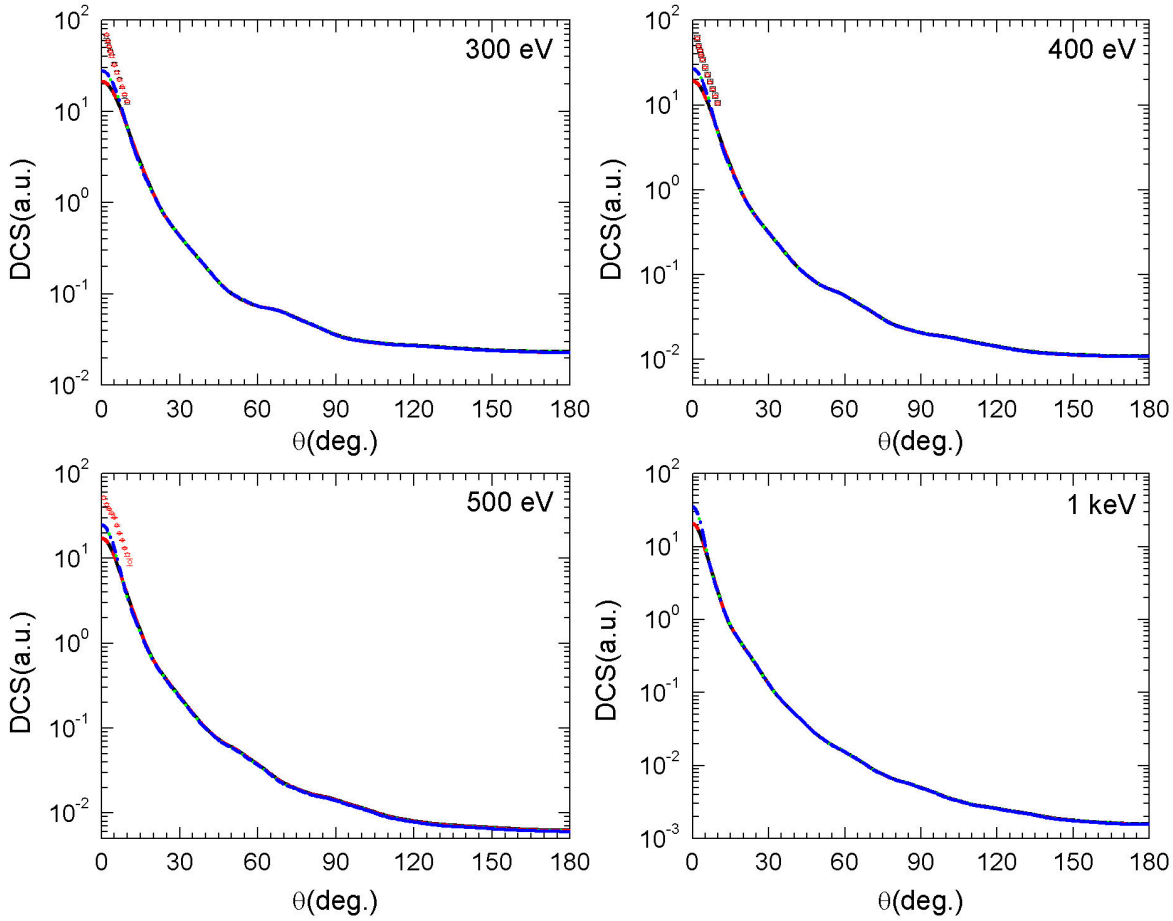

FIGURE 4. (Color on line) As in Fig. 3 at 300 eV, 400 eV, 500 eV and 1 keV. Experimental data are taken from [5] (black solid squares) and [6] (red open circles).

the amplitude is important at lower incident energies and decreases monotonically with the increasing of the impact energy. In addition, the four calculated ICSs exhibit a good agreement at intermediate and high incident energies. In fact, the little discrepancies observed at low energies ($\lesssim 30$ eV) are undoubtedly due to the exchange and polarization effects since the ammonia molecule is a polar one with a dipole moment equal to 1.42 D. We can conclude here that the polarization-correlation and exchange phenomena have perceptible effects only at lower incident energies. We have also reported in Fig. 5a) the experimental data to compare with. Note that the available measurements in the literature concern essentially the total (elastic + inelastic) cross sections, see for example Refs. [7,11,13,14]. Other experimental results are available in the literature but not reported since they are out of the energy range investigated here. First, note that some disagreements are observed in the experimental results as already mentioned by different authors [19,26]. Besides, a simple comparison with our results shows that the predicted ICSs reproduce well the shape of the measures. Concerning the magnitude, the calculated ICSs with the potential combinations $V_{st}(r) + V_{cp1}(r) + V_{ex2}(r)$ (dashed red line), and $V_{st}(r) + V_{cp1}(r) + V_{ex2}(r)$ (dash-and-dotted blue line) are in better agreement with the experimental data of Alle *et al.* [12] (black full squares) and those of Sueoka *et al.* [7] (magenta open circles). At high energies, all the calculated ICSs are in satisfactory agreement with the available measurements except that reported by Garcia and Manero [13] (black full circles). Besides, the calculated ICSs seem slightly lesser than the experimental ones in magnitude over all the energy range since the latter include the elastic and inelastic contribution (rotational and/or vibrational).

The obtained cross sections (thick lines) using different potentials are also reported in Fig. 5b where they are compared to the theoretical results existing in the literature (thin lines) taken from [21] (solid red line and dashed dotted dark-yellow line), [26] (dashed blue line), [27] (dotted magenta line and short dashed purple line), and [31] (dashed dotted-dotted pink line). Note that the shapes of all the different cross sections (thin lines) are identical with that calculated in this work (thick lines). However, the magnitudes of our CSs are, in general, lesser than the former except that of Jain [21] (solid red line). In fact all the different previous CSs include the inelastic contribution except that of Jain [21] where the elastic CSs are considered in the static-exchange-polarization (SPE) model. Finally, it is worth noting that the CSs reported

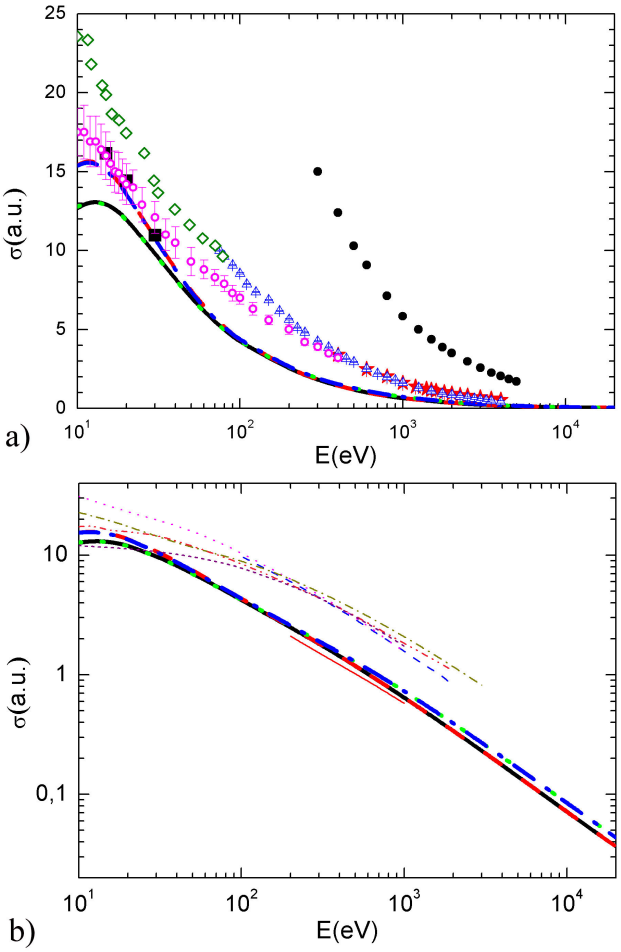

FIGURE 5. a) (Color online) Comparison between calculated ICSs for electron elastic scattering by ammonia for various potential combinations: $V_{st}(r) + V_{cp1}(r) + V_{ex1}(r)$ (solid black line), $V_{st}(r) + V_{cp1}(r) + V_{ex2}(r)$ (dashed red line), $V_{st}(r) + V_{cp2}(r) + V_{ex1}(r)$ (dotted green line) and $V_{st}(r) + V_{cp2}(r) + V_{ex2}(r)$ (dash-and- dotted blue line). Experimental data are taken from [12] (black solid squares), [7] (magenta open circles), [11] (blue up triangles), [14] (red stars), [13] (solid black circles), and [8] (olive diamonds). b) (Color online) As in Fig. 5a. Thin lines are theoretical results taken from [21] (red solid line and dark-yellow dashed dotted line), [26] (dashed blue line), [27] (dotted magenta line and short dashed purple line) and [31] (dashed-dotted-dotted pink line).

by Jain [21] including the absorption part (dashed-dotted dark yellow line) are higher in magnitude than that obtained in this work confirming in this way these arguments.

4. Conclusion

In the present work the interactions of electron with ammonia molecule are investigated and the differential and integral cross sections are calculated for the elastic scattering in the partial wave formalism. The target molecular state has been described by means of a single-center molecular wave function, while the interactions by means of complex optical potentials including a static contribution - numerically obtained, here, from quantum calculations - and fine effects like correlation, polarization and exchange phenomena rigorously selected from the literature.

The obtained DCSs for different potentials investigated show clearly the role played by the correlation, polarization and exchange phenomena particularly at lower scattering angles and lower incident energies. The calculated DCSs have shown good agreement with the experimental data both in shape and magnitude, demonstrating in this way the power of the developed model, particularly at intermediate and higher energies.

In addition, the integral cross sections calculated from 10 eV to 20 keV for different combinations of potentials investigated here show clearly a good agreement except at lower energies ($\lesssim 30$ eV) where the effects of correlation, polarization and exchanges potentials are important, confirming in this way our concluding remarks in the case of the DCSs. These results can help us to select and recommend better expressions from that investigated. In this context, it is worth noting that new experimental works are highly encouraged in order to check the ability of our theoretical approach to model the electron elastic scattering process at the total and differential scales.

1. A. L. Broadfoot, *Science* **24** (1979) 979.
2. A. Cutgian, ans S. Trajmar, *Swar studies, and Inelastic electron-molecule collisions*, Ed. L. C. Pichtford, and B. V. McKoy, (New-York 1987).
3. T. Sato, F. Shibata, and T. Goto, *Chem. Phys.* **108** (1986) 147.
4. E. Brüche *Ann. Phys., Lpz.* **1** (1929) 93.
5. W. R. Harshbarger, A. Skerbele, and E. N. Lassettre, *J Chem. Phys*. **54** (1971) 3784.
6. J. P. Bormberg, "*unpublished work*" as reported by Harshbarger *et al*. in [5].
7. O. Sueoka, S. Mori, and Y. Katayama, *J. Phys. B: At. Mol. Phys.* **20** (1987) 3237.
8. C. Szmytkowskit, K. Maciag, G. Karwasz, and D. Filipović, *J. Phys. B: At. Mol. Opt. Phys.* **22** (1989) 525.
9. H. P. Pritchard, M. A. Lima, and V. McKoy, *Phys. Rev. A* **39** (1989) 2392.
10. T. W. Shyn, "*unpublished work*" as reported by Pritchard *et al.* in Ref. 9.
11. A. Zecca, G. P. Karwasz, and R. S. Brusa, *Phys. Rev. A* **45** (1992) 2777.

12. D. T. Alle, R. J. Gulley, S. J. Buckman, and M. J. Brunger, *J. Phy. B: At. Mol. Opt. Phys* **25** (1992) 1532.
13. G. García and F. Manero, *J. Phys. B: At. Mol. Opt. Phys*. **29** (1996) 4017.
14. W.M. Ariyasinghe, T. Wijeratne, P. Palihawadana, *Nucl. Instrum. and Meth. in Phys. Res. B* **217** (2004) 389.
15. N. C. Jones, D. Field, S. L. Lunt, and J.-P. Ziesel, *Phys. Rev. A* **78** (2008) 042714.
16. A. Lahmam-Bennani, A. Duguet, and H. F. Wellenstein, *J. Phys. B* **12** (1979) 461.
17. A. Lahrnarn-Bennani, A. Duguet, H. F. Wellenstein, and M. Rouault, *J. Chem. Phys*. **72** (1980) 6398.
18. A. Duguet, A. LahmamBennani, and M. Rouault, *J. Chem. Phys.* **78** (1983) 6595.
19. G. P. Karwasz, R. S. Brusa and A. Zecca, *Riv. Nuovo Cimento* **24** (2001) 1.
20. Y. Itikawa, *J phys. Soc. Jpn* **30** (1971) 835.
21. A Jain, *J. Phys. B: At. Mol. Opt. Phys*. **21** (1988) 905.
22. M. Ben Arfa and M. Tronc, *J. Chim. Phys.* **85** (1988) 889.
23. F. A. Gianturco, *J. Phys. B: At. Mol. Opt. Phys.* **24** (1991) 4627.
24. J. Yuan and Z. Zhang, *Phys. Rev. A* **45** (1992) 4565.
25. T. N. Rescigno, B. H. Lengsfield, C. W. McCurdy, and S. D. Parker, *Phys. Rev. A* **45** (1992) 7800.
26. K. N. Joshipura and P. M. Patel, *J. Phys. B: At. Mol. Opt. Phys.* **29** (1996) 3925.
27. Y. Liu, J. Sun, Z. Li, Y. Jiang, and L. Wan, *Z. Phys. D* **42** (1997) 45.
28. G. Garcia, F. Manero, *Chem. Phys. Lett.* **280** (1997) 419.
29. J. L. S. Lino, *Rev. Mex. Fis.* **51** (2005) 100.
30. H. Munjal and K. L. Baluja, *Phys. Rev. A* **74** (2006) 032712.
31. C. Limbachiya, M. Vinodkumar, and N. Mason, *Phys. Rev. A* **83** (2011) 042708.
32. I. Shimamura, *Sci. Pap. Inst. Phys. Chem. Res. (Jpn.)*, **82** (1989) 1.
33. M. Hayashi, Electron Collision cross-sections, *Handbook on Plasma Material Science*, **4** (1992) 9.
34. W. L. Morgan, *International Symposium on Electron-Molecule Collisions and Swarms*, Tokyo, edited by Y. Hatano *et al*., (Tokyo 1999).
35. R. Moccia, *J. Chem. Phys*. **40** (1964) 2176.
36. A. Messiah, *Quantum Mechanics*, **Vol. 1 & 2**; ch 9, 10, 19, J. Wiley & Sons Inc., New York (1968).
37. R. Moccia *J. Chem. Phys.* **40** (1964) 2164.
38. J. C. Slater, *Quantum Theory of Atomic Structure*. **Vol. 2**, McGraw-Hill, New-York, (1960).
39. H. Trygve, P. Jorgensen, and J. Olsen, *In Molecular Electronic-Structure Theory*, John Wiley Sons, Inc., (2000).
40. V. Spirko, H. G. Aa. Jensen, and P. Jorgensen, *Chem. Phys.* **144** (1990) 343.
41. M. H. Mittleman and K. M. Watson, *Ann. Phys.* **10** (1960) 286.
42. A. Salvat, A. Joblonski, and C. J. Powell, *Comput. Phys. Commun.* **165** (2005) 157.
43. N. T. Padial and D. W. Norcross, *Phys. Rev. A* **29** (1984) 1742.
44. W. J. Jr Carr and A. A. Maradudin, *Phys. Rev*. **133** (1964) 371.
45. J. B. Furness, I.E. McCarthy, *J. Phys. B: At. Mol. Phys*. **6** (1973) 2280.
46. M. H. Mittleman and K. M. Watson, *Ann. Phys*. **10** (1960) 286.
47. M. E. Riley and D. G. Truhlar, *J. Chem. Phys*. **63** (1975) 2182.
48. H. Aouchiche, F. Medegga, and C. Champion, *Nucl. Instr. Meth. Phys. Res. B* **333** (2014) 113.
49. F. Medegga, H. Aouchiche, *High Energ. Chem.* **51** (2017) 462.
50. L. M. Brescansin, L. E. Machado, M-T Lee, H. Cho and Y. S. Park, *J. Phys B: At. Mol. Opt. Phys.* **41** (2008) 185201.
51. H. Cho, R. P. McEachran, S. J. Buckman, and H. Tanaka, *Phys. Rev. A* **78** (2008) 034702 and references therein.